Journal of Hydrology 562 (2018) 346–357

Contents lists available at ScienceDirect

Journal of Hydrology

journal homepage: www.elsevier.com/locate/jhydrol

Research papers

The bridge between precipitation and temperature – Pressure Change Events: Modeling future non-stationary precipitation

Ziwen Yu[a,*], Stephanie Miller[a], Franco Montalto[a], Upmanu Lall[b]

[a] Civil, Architecture and Environmental Engineering Department, Drexel University, Curtis 251 3141 Chestnut Street, Philadelphia, PA 19104, USA
[b] Department of Earth & Environmental Engineering, Columbia University, 500 West 120th Street 918 Mudd, New York, NY 10027, USA

ARTICLE INFO

This manuscript was handled by Marco Borga, Editor-in-Chief, with the assistance of Francesco Marra, Associate Editor

Keywords:
Precipitation analysis
Weather type categorization
GCM temperature
Hourly precipitation
Average monthly temperature
Pressure change event
Probability of precipitation
Extreme event

ABSTRACT

Anthropogenic warming may change precipitation patterns, impacting infrastructure performance and reliability. Future precipitation statistics generated using General Circulation Models (GCM) are, however, often biased and not easily applied to problems such as runoff estimation. Stochastic weather generation is hence used as an alternative to GCMs in hydrology and hydraulic modelling. This paper explores the dependence of fine temporal precipitation characteristics on air pressure and air temperature using historic observations. The goal is to develop, based on the key causes of precipitation, a climatological basis for a stochastic precipitation generator for non-stationary precipitation under climate change conditions. The analysis focuses on precipitation in the urban Northeast United States and utilizes pooled observations from meteorological stations in New York City, Philadelphia, and Boston over 60 years. A negative correlation between hourly Probability of Precipitation (POP) and air pressure is observed. When the historical records are discretized using air Pressure Change Events (PCE), Decreasing Pressure Change Events (DePCEs) had a higher POP and a higher Precipitation Depth (PD) than Increasing Pressure Change Events (InPCEs). Temperature was more strongly associated with PD during DePCEs than InPCEs; this association was more pronounced during high magnitude PCEs and extreme events. The potential for simulating future hourly precipitation by associating historic hourly precipitation patterns with PCE's and monthly temperature is assessed.

1. Introduction

Global climate variability and change is largely caused by modifications to the global energy and water cycles. To improve our ability to adapt to precipitation changes under global warming (Trenberth et al., 2003), research is necessary to characterize the relationship between precipitation and temperature (Trenberth, 1998; Trenberth et al., 2003; Allan and Soden, 2007; Neiman et al., 2008; Lenderink and van Meijgaard, 2010). This relationship is complex, as it varies over space and time. Although General Circulation Models (GCMs) can generally investigate coarser temporal scales (e.g. annual or decadal) in larger geographic areas (e.g. Northeast US, global), more uncertainties are observed at smaller temporal and spatial scales, since local climate is also influenced by local geography, land cover, and related circulation patterns (Mitchell et al., 1999; Räisänen, 2001; Zveryaev and Allan, 2005; Sorteberg and KvamstØ, 2006).

Researchers have tried to link these two factors using physical and atmospheric explanations. For example, Trenberth et al. (2003) suggested that through convection, the moisture required for precipitation is drawn from an area of atmosphere that is about four times the rainy area. A 7% increase in air moisture holding per degree of warming at the local level has been used to imply a similar rate of global precipitation change, based on the Clausius–Clapeyron relation (Trenberth and Shea, 2005; Sun et al., 2007). Other studies investigate this relationship at different time scales, from monthly (Trenberth and Shea, 2005; King et al., 2014) to daily (Sun et al., 2007; Westra et al., 2013) and sub-daily (Lenderink and van Meijgaard, 2008, 2010); still others explore this relationship based on differences in precipitation patterns, looking at means (Allen and Ingram, 2002; Trenberth, 2011), extremes (Groisman et al., 2005; Meehl et al., 2005; Shaw et al., 2011; Meehl et al., 2012; Kunkel et al., 2013), and events of varying durations (Panthou et al., 2014; Wasko et al., 2015b).

For example, Madden and Williams (1978) found a frequent negative correlation between precipitation and summer air temperature at time scales ranging from inter-annual to multi-decadal in the contiguous United States and Europe. Zhao and Khalil (1993) confirmed a similar negative correlation in the summer, after exploring monthly data of the contiguous United States from 1905 to 1984. However, on

* Corresponding author.
E-mail address: zy32@drexel.edu (Z. Yu).

https://doi.org/10.1016/j.jhydrol.2018.05.014
Received 28 February 2018; Received in revised form 4 May 2018; Accepted 5 May 2018
Available online 08 May 2018
0022-1694/

days with mean daily temperatures in excess of 12 °C, Lenderink and van Meijgaard (2008) found that the probability of one-hour precipitation extremes in De Bilt, Netherlands increased much faster than the Clausius–Clapeyron relation suggests, extending this finding to larger European simulations.

In general, projections from GCMs are used to interpret the relationship between precipitation and temperature at coarser temporal scales (e.g. annual or decadal) under climate change scenarios when considering larger geographic areas (e.g. Northeast US, global). Yet, precipitation datasets at fine time scales (e.g. hourly or sub-hourly) are required to study the potential impacts of climate change on water resource management, urban hydrology, and agriculture. For example, one of the two primary causes of runoff is Hortonian excess precipitation, whereby runoff is generated instantaneously whenever the intensity of precipitation exceeds the infiltration capacity of the land surface. To assess whether precipitation will be more intense under climate change, and possibly increase runoff generation, precipitation sequences downscaled from GCM projections are needed at fine temporal scales. Despite the dynamic methods used by Regional Climate Models (RCMs), stochastic precipitation generators, based on downscaled GCM projections, have been developed as an alternative (Fowler et al., 2007; Wilks, 2010) and used extensively for flood risk management (Haberlandt et al., 2008), sizing reliable rainwater harvesting systems (Basinger et al., 2010), and other water resource management tasks (Shamir et al., 2015). Stochastic precipitation generators create long continuous Markovian sequences of precipitation through a variety of methods (Wilks and Wilby, 1999). One technique for sequence generation uses samples from parameterized statistical distributions of wet-day rain volume (Stern and Coe, 1984; Wilks, 1998), arrival and cell conditions intensity and duration (Rodriguez-Iturbe et al., 1987, 1988; Wasko et al., 2015a; Wasko and Sharma, 2017), and event characteristics (Heneker et al., 2001); another relies on non-parametrically sampling historical observations (Lall et al., 1996; Lall and Sharma, 1996; Sharma and Lall, 1999; Basinger et al., 2010) with a moving window to preserve seasonality (Rajagopalan et al., 1996).

The quality of downscaled GCM precipitation datasets is contingent upon accurate temperature predictions and a strategy for minimizing prediction bias (Johnson and Sharma, 2009; Johnson and Sharma, 2012). Researchers found that pressure and temperature have the most agreement across the GCMs (Johnson and Sharma, 2009), while precipitation has the least consensus(Kendon et al., 2008; Johnson and Sharma, 2009). A better understanding of the relationship between precipitation and temperature is necessary to increase confidence in precipitation projections derived from other GCM projections, such as monthly temperature.

This paper explores how fine temporal scale (e.g. hourly) precipitation patterns are related to coarser temporal scale (e.g. average monthly) temperature. The physical causes of precipitation in a free atmosphere system are discussed first. Next, an investigation into the relationship of air pressure and precipitation is explored both at hourly time steps, and on an event basis. This analysis is then extended to examine how event based precipitation characteristics are impacted by Average Monthly Temperature (AMT). The results are used to discuss the potential development of a new stochastic precipitation generator that produces synthetic hourly precipitation time series by non-parametrically resampling historical observations, informed by GCM projections of AMT, among other variables.

2. Mechanisms of precipitation

One of the key causes of precipitation is the condensation of air that ascends as it moves laterally over irregular terrain (orographic lifting) or is physically displaced by atmospheric phenomena (e.g. via frontal lifting) (Bjerknes and Kristiania, 1922). Condensed moisture then falls to the ground as precipitation after drops coalesce enough to overcome the forces of drag (Ahrens et al., 2012).

In a free atmosphere, the primary cause of condensation is the displacement of air masses (Bjerknes and Kristiania, 1922). The earliest researcher describing precipitation generated from the frontal movement of air masses was Bjerknes and Kristiania (1923), who studied atmospheric circulation patterns. There are three main categories of frontal precipitation (Bjerknes and Kristiania, 1922; Bjerknes and Kristiania, 1923): (1) A cold front forms when cold, dry stable air masses lift and replace relatively unstable, warm, moist air masses previously found near the land surface. Typically, the cold air moves from the northwest to southeast direction in the northern hemisphere. The cold air forces its way under the warm air, which is then convected upward, where it cools, condenses, and coalesces, often causing short-duration, high-intensity precipitation. (2) By contrast, a warm front is formed by the advance of a warm moist air mass and the simultaneous slow retreat of cold dry air. Most commonly, warm air moves from the southeast to the northwest in the northern hemisphere. Since warm air has a lower density, it rolls up and over the cold air and can cause light to moderate precipitation over a large geographic area. (3) Occludal fronts occur when cold and warm fronts collide, causing a cyclone with low pressure in the joint area. Occludal fronts typically move to the northeast, and cause synoptic (because both warm and cold fronts are present) precipitation over large land areas. Fig. 1 graphically illustrates the three types of fronts.

Ahrens et al. (2012) summarized general relationships between precipitation, temperature, and pressure for each of the three types of fronts (Table 1). Note that the trends in temperature changes are not consistent for all front types, especially for the Occludal front, which makes it difficult to develop a direct relationship between temperature and precipitation. However, when air is lifted by any of the three different frontal mechanisms, air pressure at the ground surface is

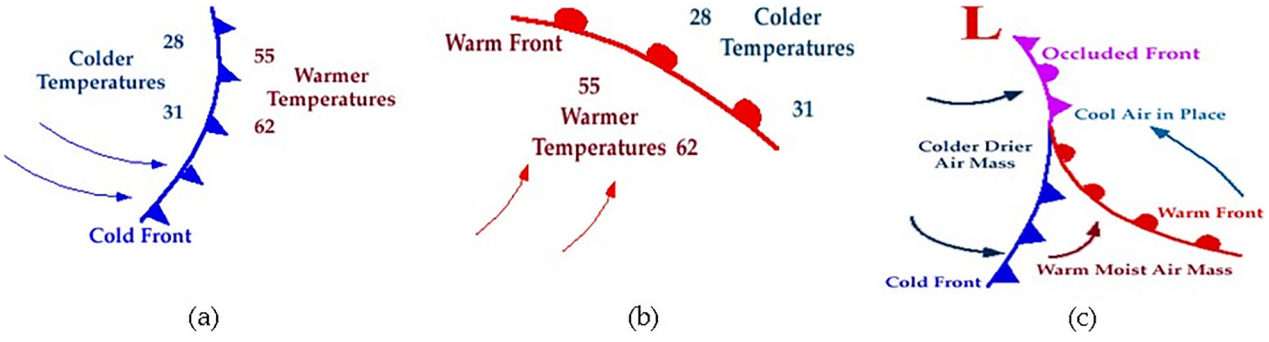

Fig. 1. Air mass front types (the numbers in plot indicate temperature in Fahrenheit) (a) Cold front, blue arrows indicate the direction of movement, (b) Warm front, red semi-cycles indicate the direction of movement, (c) Occludal front, purple arrows and semi-cycles show the direction of move, both cold front and warm front move counter-clockwise and produce low pressure region in the joint area. (Urbana-Champaign, 2010). (For interpretation of the references to colour in this figure legend, the reader is referred to the web version of this article.)

Table 1
Climate characteristic effect of three front types a) Cold front, b) Warm front, c) Occludal front (Urbana-Champaign, 2010).

		Before Passing	While Passing	After Passing
(a)	Temperature	Warm	Sudden drop	Steadily dropping
	Pressure	Falling steadily	Minimum, then sharp rise	Rising steadily
	Precipitation	Short period of showers	Heavy rains, sometimes with hail, thunder and lightning	Showers then clearing
(b)	Temperature	Cool-cold, slow warming	Steady rise	Warmer, then steady
	Pressure	Usually falling	Leveling off	Slight rise, followed by fall
	Precipitation	Light-to-moderate rain, snow, sleet, or drizzle	Drizzle or none	Usually none, sometimes light rain or showers
(c)	Temperature			
	• Cold occluded	Cold or cool	Dropping	Colder
	• Warm occluded	Cold	Rising	Milder
	Pressure	Usually falling	Low point	Usually rising
	Precipitation	Light, moderate, or heavy precipitation	Light, moderate, or heavy continuous precipitation or showers	Light-to-moderate precipitation followed by general clearing

consistently reduced (Hughes and Mayes, 2014). This phenomenon is well-documented at the synoptic scale, as a result of frontal precipitation (Urbana-Champaign, 2010). At the local or *meso*-scale, Hoxit et al. (1976a,b) found that surface pressure dropped due to the formation of convective clouds, triggering showery storms. The magnitude of the pressure drop is associated with the type of air mass movement at the synoptic scale or with the extent of the surface heating imbalance at the meso-scale, suggesting that in both cases pressure changes may provide a potential physical link between precipitation and seasonal variable frontal movements, related to AMT and atmosphere stability.

3. Data and methods

3.1. Data

The analysis focuses on the northeastern coastal United States, a region extending from Philadelphia to Boston, and characterized by plains with no high mountains. In this region, other than the general surface heating mechanism for local summer storms, the vertical movement of air masses is typically associated with frontal precipitation, rather than orographic lifting. Studies describing the relationship between precipitation and temperature (Lenderink and van Meijgaard, 2010; Shaw et al., 2011; Panthou et al., 2014; Wasko and Sharma, 2017) use data from many locations to prove the geographical representative of their statistics. However, the physical mechanism of precipitation formation in this study area has been observed in many other locations around the world (Hoxit et al., 1976a,b; Knupp and Cotton, 1985; Neiman et al., 2008; Adams-Selin and Johnson, 2010; Ahrens, 2012; Dawn and Mandal, 2014; Houze et al., 2015). The data used in this study includes hourly observations of temperature, sea level air pressure, and precipitation from the international airports in New York City, Philadelphia and Boston from 1948 to 2011.

Since the topography and climate across the region are known to be similar, data from the three cities, spanning over a distance of 480 km, are pooled for this analysis. More frequent extreme precipitation in the future has been projected for this region by other researchers (Hayhoe et al., 2008; Demaria et al., 2016; USGCRP, 2017). The pooling increases the number of data points that can be used in the analysis, especially for the extremes.

Because 1.04% of all time steps in the historical data contains some gaps, (i.e. missing data, cumulative period with no detailed information, the time-interval of observation is longer than one hour for several decades, etc.), an interpolation method is developed to fill in the missing data points for gaps less than 24 h. A moving average method, with a window width of a single day, is used to smooth out gaps of less than six hours (1.03%). For gaps between six hours and 24 h (0.01%), a 2nd harmonic function is fitted to the values of the dry days (all gaps are treated as dry), with a length of one week (adjustable) centered on the day of interest and adjusted to match the values of the gap's end points. Then, using this adjusted harmonic function, the gaps were filled with values that mimic the general change pattern for the neighboring days and which connect smoothly to the observed data. Fig. 2 illustrates a sample of such a case. This method is applied on both temperature and air pressure. Where longer gaps (> 24 h) were evident, data was eliminated from the analysis.

3.2. Methods

Because the movement of air masses is typically associated with pressure changes, the first step in the analysis was to investigate the pressure changes associated with precipitation. For the purposes of this paper, both pressure change and precipitation were investigated on an

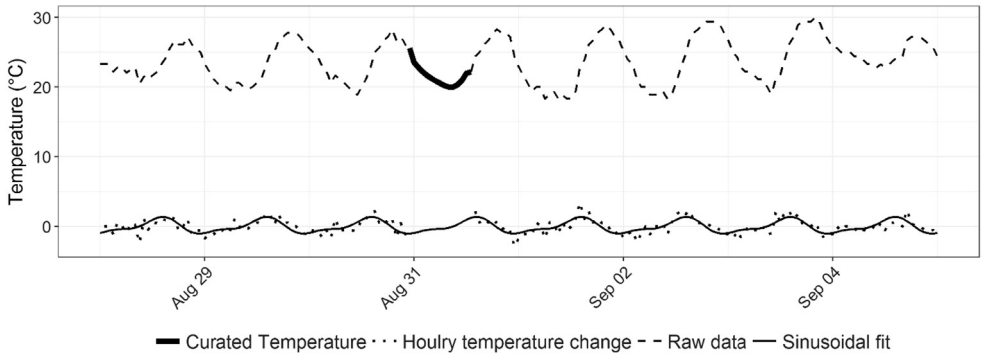

Fig. 2. Sample of missing data filling.

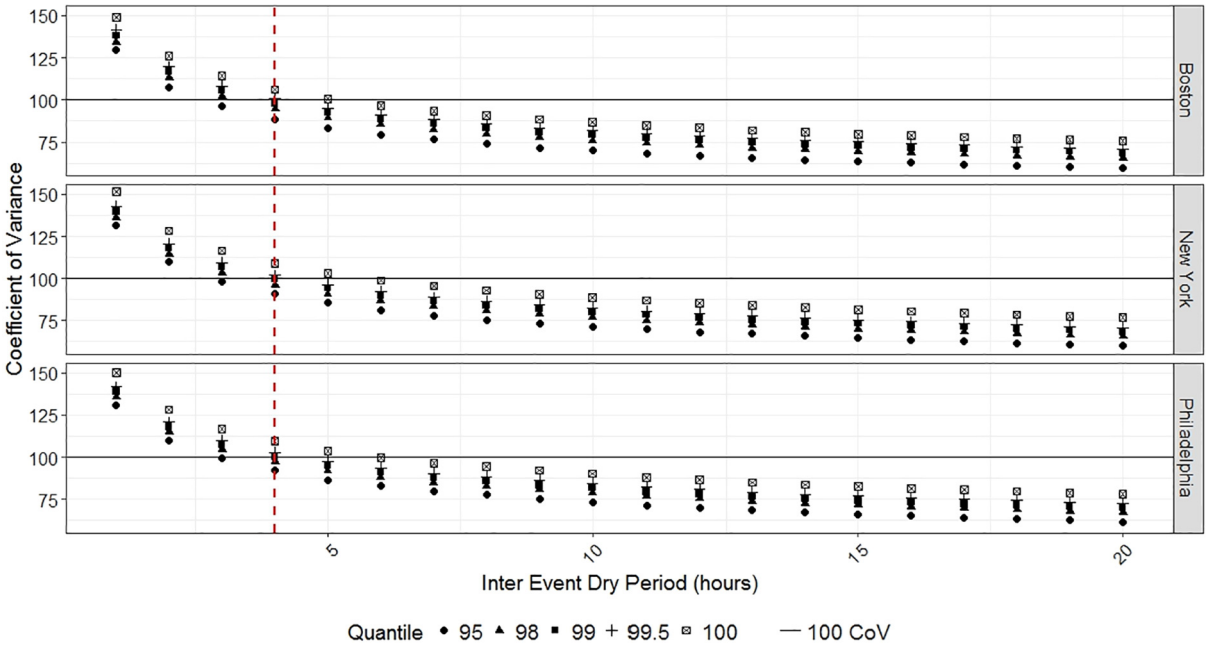

Fig. 3. Analysis of IntEDP, black horizontal solid line (CV of unity), red vertical dash line (4 h IntEDP).

event basis. Precipitation events were defined by an Inter-Event Dry Period (IntEDP). Based on Restrepo-Posada and Eagleson (1982), IntEDP follows an exponential distribution for which the mean equals the standard deviation, or Coefficient of Variation (CV) of unity. However, the historic IntEDP is affected by extreme events, which dramatically affect calculations of the CV. In Fig. 3, the CV for each city is calculated and plotted based on IntEDP quantile thresholds of 95%, 98%, 99%, 99.5% and 100%. An IntEDP beyond each threshold is not included in the calculations. Based on the results, the CV is sensitive to the extreme events in the distribution tail (e.g. the 100% results are far from 99.5% results, especially for the short IntEDPs). To avoid the influence of these low-frequency events (e.g. 0.5% for 99.5% quantile threshold), this paper uses 99.5% as the quantile threshold to determine the minimum IntEDP, which is four hours for all cities (Fig. 3).

A Pressure Change Event (PCE) is defined using de-seasonalized air pressure. De-seasonalized air pressure is the change in air pressure over a 24-h period, as shown in the following equation.

$$P'(t) = P(t) - P(t-24)$$

where P(t) is the actual air pressure on hour t, P'(t) is the de-seasonalized air pressure on hour t. Two different types of PCEs are possible, as shown conceptually in Fig. 4. The horizontal axis represents time, while vertical axis represents the change in air pressure over 24 h, i.e. the de-seasonalized air pressure series. The shaded areas above the horizontal axis are defined as an Increasing Pressure Change Events (InPCEs) because the air pressure increases over time. The shaded areas below the horizontal axis are defined as Decreasing Pressure Change Events (DePCEs), because air pressure decreases with time. The local maxima and minima in the figure indicate the greatest positive and negative 24-h changes in pressure, respectively. As shown in Fig. 4, each PCE, increasing or decreasing, is bracketed by time points of stable pressure (e.g. no change over 24 h). Using the data in this study, InPCEs correspond to Event Pressure Changes (EPC) from 0 to 1100 hPa; DePCE EPCs range from −1200 to 0 hPa. EPC is defined as the cumulative air pressure change within a PCE. The sample sizes of PCEs for BOS, NYC and PHL were, respectively, 11,564, 7147 and 8511. Based on the meteorology finding described in Table 1, precipitation is hypothesized to occur more frequently during DePCEs.

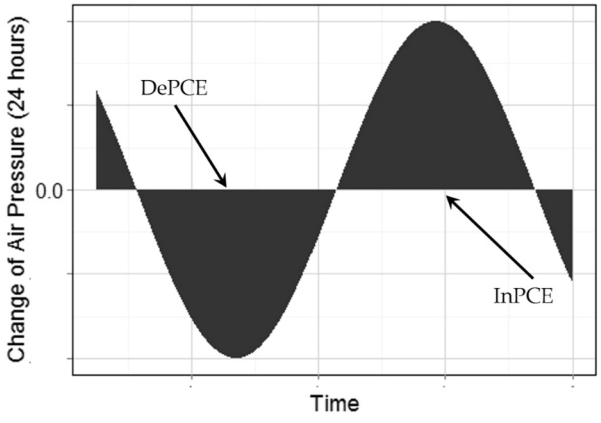

Fig. 4. PCE definition.

Next, the relationships between historical hourly precipitation and air pressure were explored. An exploratory analysis was performed to determine whether air pressure is related to precipitation across the study area. Hourly Probabilities of Precipitation (POPs) over the full air pressure range for a year and each month were explored graphically. Then, the association between precipitation occurrence and pressure change was qualitatively investigated on an event basis. Historical observations were specifically inspected for coincidences of DePCEs and precipitation. An EPC histogram of both rainy and non-rainy PCEs was plotted to explore whether precipitation is more frequently triggered during DePCEs. The association between precipitation and EPC was then further analyzed and quantified in terms of PCE Precipitation Depth (PD) and PCE POP, with both computed from the total number of rainy PCEs.

For the association between precipitation and PCE to be applicable under climate change conditions, it is hypothesized that atmosphere stability, PCE POP, and PCE PD must be dependents of AMT. To test this theory, the frequency of PCEs is graphically inspected to interpret the stability of atmospheric system under different AMT conditions. By importing AMT information, the seasonality, corresponding PD, and POP of different PCE types is explored. To bridge precipitation and AMT, heatmaps and contours of PCE POP were overlaid with AMT for different half-years (Jan – June and July – Dec); different PCE PD percentiles were also investigated against AMT under different EPC

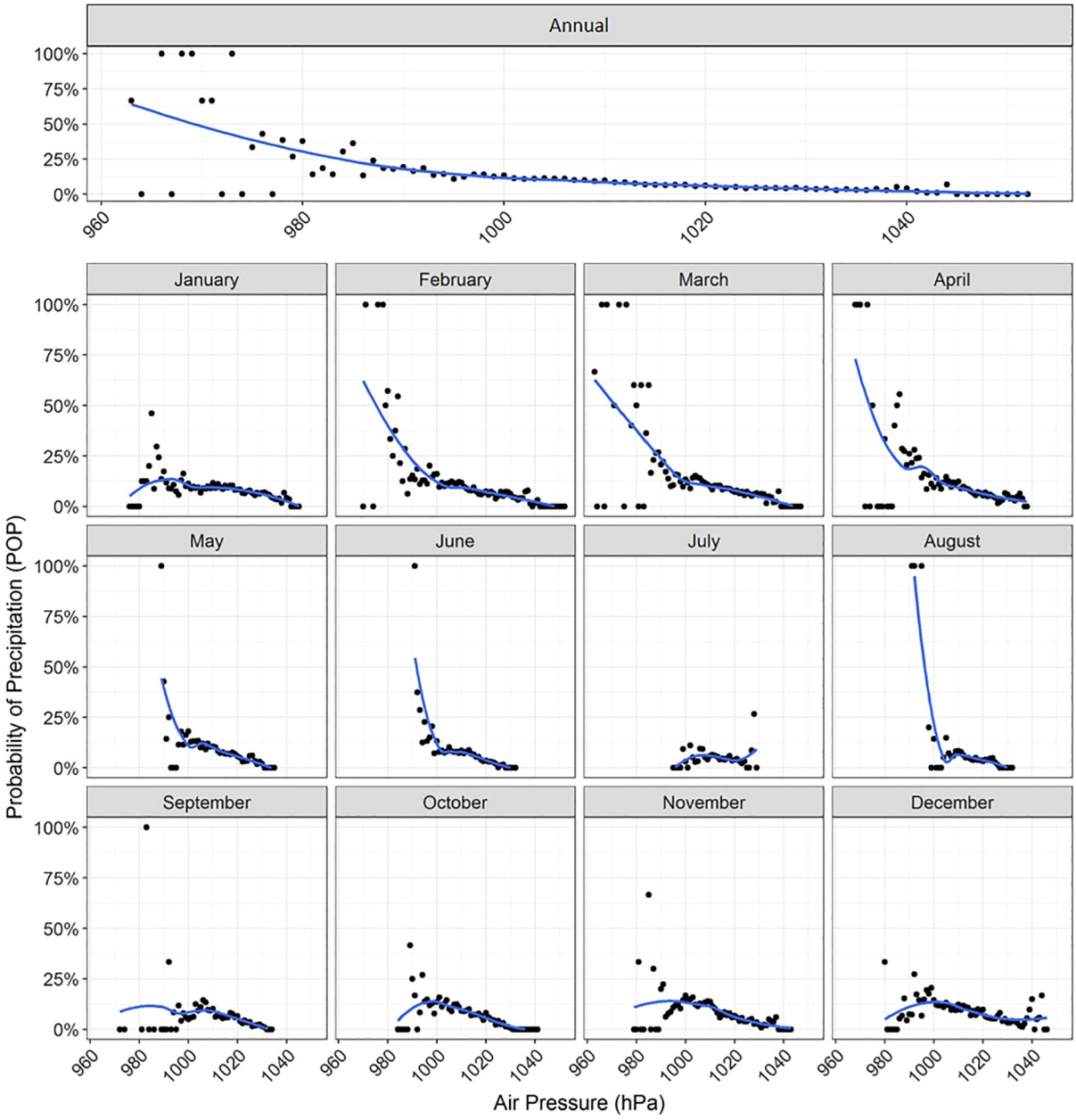

Fig. 5. POP on hourly air pressure in NYC LaGuardia International Airport (the local regressions are indicated by the blue lines). (For interpretation of the references to colour in this figure legend, the reader is referred to the web version of this article.)

magnitudes and seasons.

4. Results and discussion

Fig. 5 displays POP associated with different air pressures for LaGuardia International Airport (NYC) at an hourly time scale. POP in this chart refers to the probability of any form of precipitation. At the top of the chart is the POP versus hourly air pressure for the full data set. Below, POP is broken down by month. The figure indicates that POP is negatively correlated to the hourly air pressure, irrespective of month. However, during July, August, and September, this trend is less pronounced than during other months. This trend is likely because 1) the air system is relatively stable in summer, with less variability in air pressure, and 2) summertime convection storms are often highly localized and may not pass over the climate station, even it is in the tributary area of the storm's convection. The same trends and phenomena were also found in Boston and Philadelphia (Figures not shown).

Fig. 6 shows a sample sequence of alternating PCEs (shaded area) and the associated hyetographs (bars) and 24-h-smoothed temperature (line). This graph illustrates that precipitation is generally associated with the DePCEs, which supports the trends illustrated in Table 1 (i.e. that frontal precipitation is successive to pressure fall).

Histograms describing all pooled PCEs and all rain-triggering PCEs are shown in Fig. 7. The rain-triggering PCEs are defined as those PCEs whose durations overlap with the beginning of a precipitation event. The histogram of the full sample of all PCEs is similar to a normal distribution, with a mean near zero. The distribution of rain-triggering PCEs is, however, skewed to the left and is discontinuous at the vertical axis (in the negative range). The left-skewness is consistent with the meteorological interpretation that as air masses are vertically lifted, negative changes in pressure are associated with precipitation events. The discontinuity in the distribution could indicate the presence of two different types of fronts. Cold fronts lift warm air rapidly, generating precipitation over relatively small geographic areas very soon after the

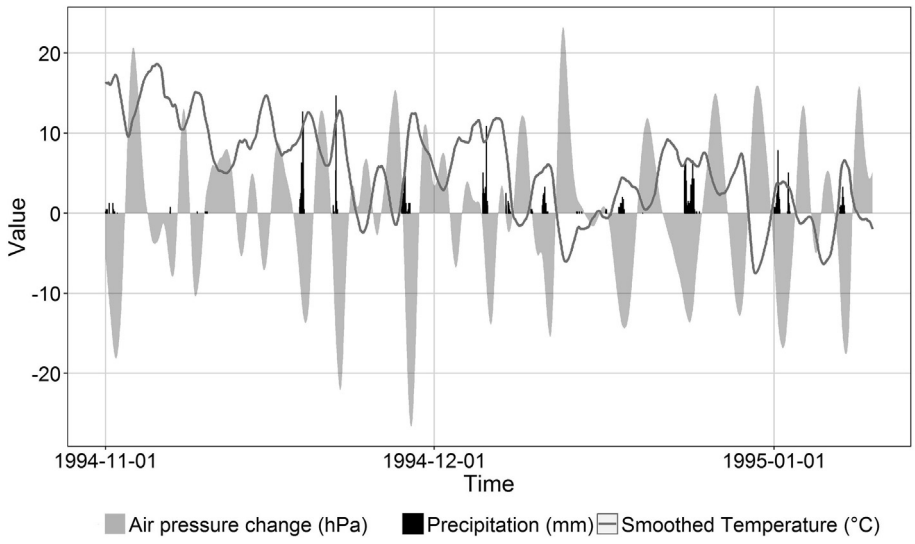

Fig. 6. PCEs and precipitation from 1994 to 11-01 to 1995-1-10 in BOS.

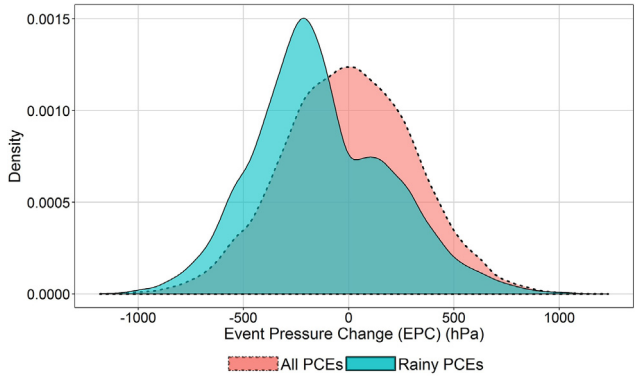

Fig. 7. Kernel density of EPC for rain triggered PCEs (green) and all PCEs (red). (For interpretation of the references to colour in this figure legend, the reader is referred to the web version of this article.)

pressure drops. Because POP in the negative region of Fig. 7 is higher, it may be that these events correspond to cold-front storms. Alternatively, the smaller POP under positive EPC may correspond to warm-front storms, since warm-front storms usually affect a large region ahead of the front. For this reason, precipitation correlated with InPCE has a lower POP.

The POP and PD associated with EPCs are depicted graphically in Fig. 8. A local fit line (dashed) using loess method (Cleveland et al., 1992) is used to highlight the correlation between POP and EPC. Note, the density plot in the lower chart reflects only the distribution of the rainy PCEs, as all dry PCEs are all laying atop the x axis (PD = 0 mm). Two distinct PCEs are divided by EPC = 0 hPa. As the absolute value of an EPC increases, the POP of DePCEs increases from 15% to 100% within 0 ~ −300 hPa, while InPCE POP increases only from 15% to about 40% within 0–820 hPa. Given that the sample size of intensive InPCEs is limited (n = 79 when EPC > 820 hPa), less confidence is associated with the POP beyond 820 hPa. Falling pressure appears to be a better indicator of precipitation than increasing pressure. The highest PCE occurrence occurs at EPC values of approximately −250 hPa and PD of 20 mm. These ranges are consistent with the histogram shown in Fig. 7. Similar to POP, the trend of PD versus EPC can also be divided by PCE types. For DePCEs, the PD increases along with the EPC magnitude, while for InPCEs, EPC magnitude reduces PD. Physically, InPCE appears in a stable atmosphere, which does not benefit air mass lifting and so lacks the moisture supply necessary to intensify the precipitation process as DePCE does.

Bjerknes and Kristiania (1923) reported that the average lifetime of an air circulation system was 5.5 days, a period that was similar in duration to the average 5.7 days of precipitation events reported in 1909 by Defant (1921). It suggests that occurrence of air circulation and its corresponding air pressure change could be treated as an indicator of atmosphere stability, especially for moderate and intensive events. Since precipitation is formed due to atmospheric instability, it is important to evaluate the impact of temperature on the atmospheric system. The monthly frequency of moderate and intensive PCEs (absolute value of EPC > 90 hPa) is plotted in two half-years against AMT in Fig. 9, with a local regression line. An obvious negative relationship when AMT > 0 °C can be seen for both half-years. Atmospheric systems are more stable when the weather gets cold (AMT < 0 °C). This illustrates that the atmospheric system stability, indicated by monthly frequency of moderate and intensive PCEs, is a function of AMT, one of the GCM outputs. It should be noted that even though the occurrence becomes low, individually PCE in high temperature is generally more intensive than low temperature.

To further investigate the impact of AMT on PCE and its associated precipitation characteristics, Figs. 10 and 10 present the PD and POP for two halves of the year, indexed by AMT.

The relationship between PD and AMT is contoured by frequency in Fig. 10 for both InPCEs and DePCEs. Two seasonal systems (centroids), winter and summer, are visible for both PCE types. The summer system is concentrated around 8 mm for DePCEs and 6 mm for InPCEs (both centroids near 22 °C). The difference of PD between DePCE and InPCE in summer is not pronounced since precipitation tends to be localized in the relatively stable atmospheric system, as implied by the narrow variance of air pressure. However, the opposite is true for winter system. The winter system is centered around 17.5 mm for DePCEs and 2.5 mm for InPCEs (both centroids near 2.2 °C). This indicates that DePCE has a larger geographical scale effect on winter storms. The magnitude of this difference fades out as the AMT grows from winter to summer. The change in PD between winter and summer is +3.5 mm for InPCEs and −8.5 for DePCEs. These differences are largely due to the seasonality of precipitation formation, with large-scale, frontal mechanisms dominating in winter, and local air convection dominating in summer.

Fig. 11 illustrates the POP of both PCE types under different AMT conditions. The POP of DePCEs is generally higher than of InPCEs which is coincided with Figs. 7 and 8. For DePCEs, during both halves of a year, POP is roughly level, oscillating between 55% and 65% with

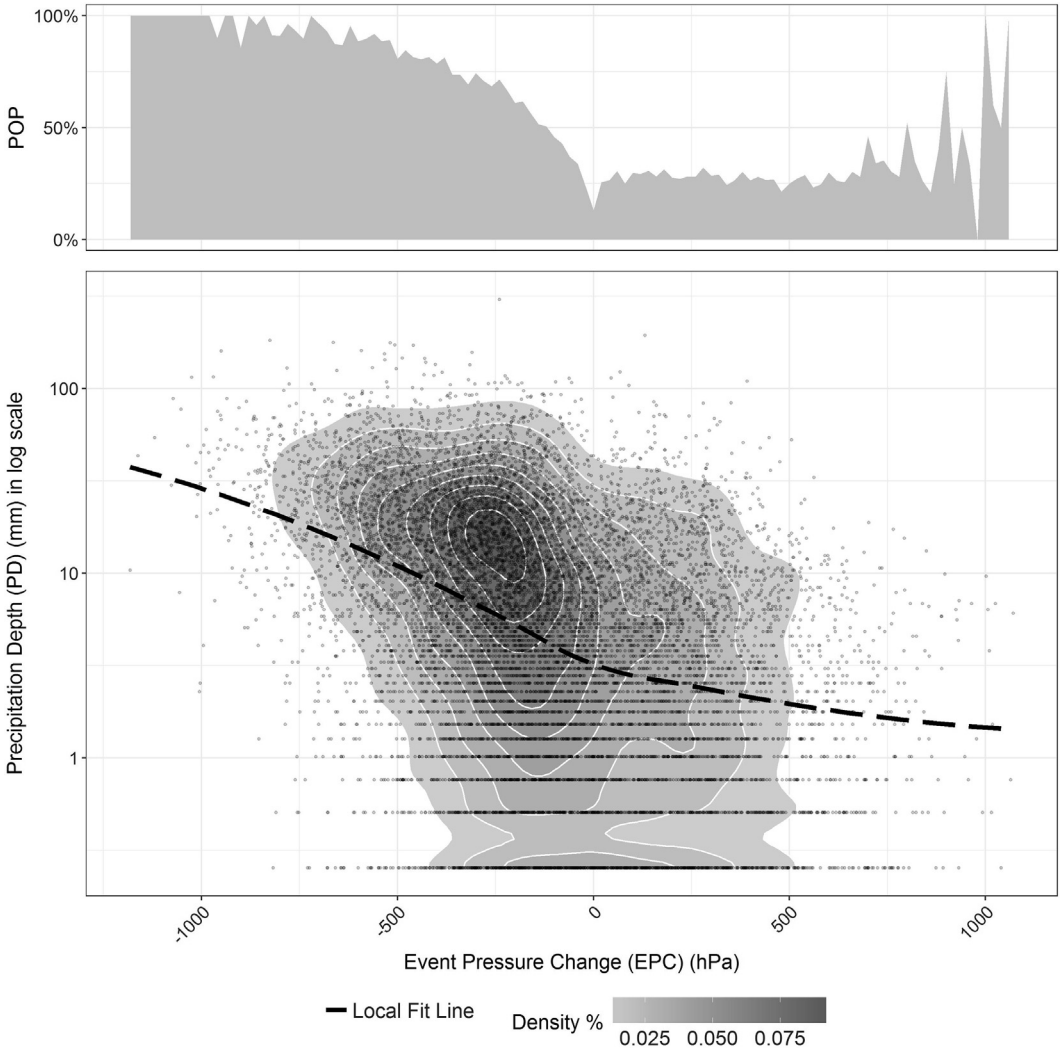

Fig. 8. Relationship between PD and POP vs. EPC.

some small differences in the tail regions (e.g. high and low end of AMT range). The small POP during low temperatures in the second half of the year (Jul ~ Dec) is not reliable, due to a limited sample size (n = 9 for both InPCEs and DePCEs). However, during high temperatures, the POP decreases about 10%. This could be another impact of meso-scale summer convection storms, which generally have a tributary area much larger than the area of precipitation (Hoxit et al., 1976a,b). Given that the data in the study is only from three airports, it is very likely these areas contribute to convections forming storms elsewhere. For InPCEs, during both year halves, the POP indicated is approximately 25% at the lowest temperatures and 35% at the highest. Between Jan and Jun, POP gradually rises to 35% between 4 °C and 10 °C, while during Jul and Dec, the increase in POP is delayed until the temperature increases from 20 °C to 26 °C. This observation suggests that the precipitation / pressure dynamics in the fall and spring differ somewhat from one another, although both have a similar temperature range (6 °C).

The PD of spring and fall are difficult to differentiate in Fig. 10, since their AMTs overlap. Similar POP values are shown in Fig. 11 for DePCEs, though the temperatures at which POP increases for InPCEs are slightly different. The increase in POP could be caused by warm-front frequency under different AMTs. Since warm air masses generally move to the north in spring, it is reasonable to expect stronger warm-front storms in spring than in the fall.

This analysis suggests that high POP in this geographical region is associated both with low absolute pressure and with DePCEs. It also indicates that PCE could serve as a potential link between AMT and POP. This relationship is plotted in Fig. 12 in terms of POP and PCE against AMT, with break points in the middle of a year. POP ranges from 0% (tan) to 100% (light blue). Generally, POP is higher in DePCEs for the entire year. As indicated by the contours of the local regression, POP for DePCEs is highest when EPC is near -800 hPa, regardless of the time of year. Between July and December, POP increases as temperatures decrease. For InPCEs, EPC magnitude is positively correlated to POP, though this correlation is more pronounced for DePCEs.

As a further investigation, we explored PD quantiles against EPC and AMT in different seasons (Fig. 13). Three PD percentiles, 50%, 75% and 95%, are included. The relationships represented by the local regression lines are colored by season. Vertically, similar to the results presented in Fig. 8, PD percentiles increases as the EPC drops, especially in DePCE regions. This generally holds for all PD percentiles and seasons. Horizontally, PD seems to vary greatly depending on the AMT, with an amplified magnitude on high percentile categories (75% and 95% quantiles). For intensive (500 hPa–2000 hPa) and non-intensive (0 hPa–500 hPa) InPCEs, the all-season dash lines reflect the overall relationship between PD and AMT since seasonality is not significant. When AMT is lower than 10 °C, PD stays small. At temperatures above 10 °C, non-intensive InPCE PD starts to increase slightly with AMT in the PD percentiles of 95%. This increase is amplified in intensive InPCEs for all PD quantiles, as shown in Fig. 13, but delayed to 22 °C, which almost exclusively represents summertime events. It should be

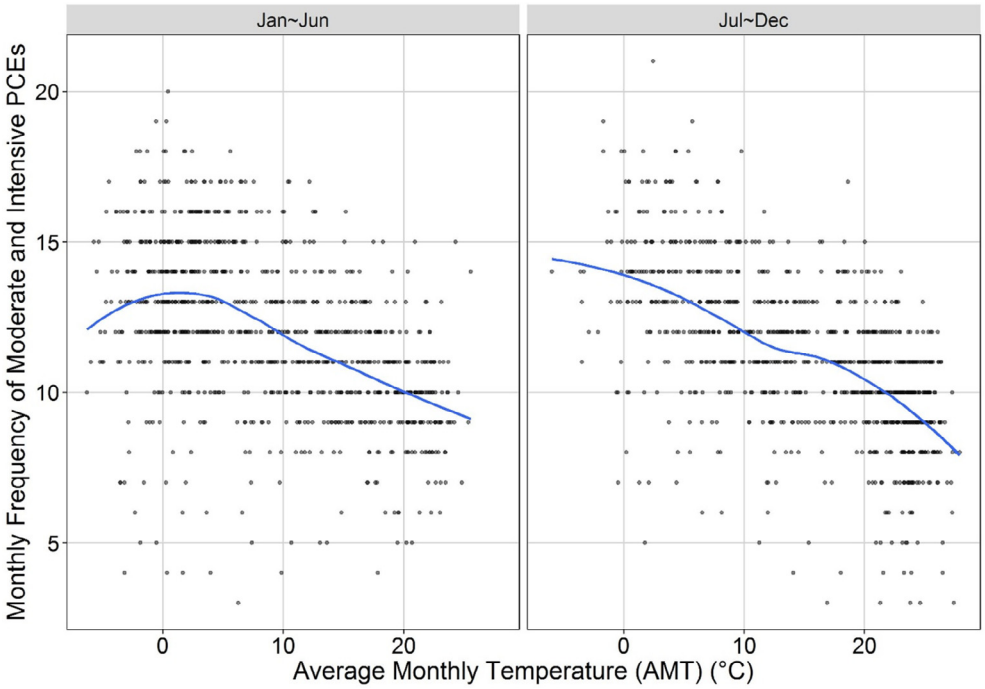

Fig. 9. Association between monthly PCE frequency and AMT with local regression line (blue). (For interpretation of the references to colour in this figure legend, the reader is referred to the web version of this article.)

noted that this amplification could be caused by the limited sample size (n = 40 for 23 °C–26 °C) at the corresponding AMT range and thus may not be reliable.

For DePCE, seasonality is more pronounced in high PD percentiles (75% and 95%) and under intensive EPC conditions. When combined with the density graph from Fig. 8, non-intensive (−500 hPa–0 hPa) DePCEs occur more frequently than other EPC categories and thus are more important in the investigation of how PD responds to PCEs and AMT. Although not all pronounced, non-intensive DePCEs generate more precipitation when AMT is higher, obvious for PD in the 95th percentile. This trend for non-intensive DePCEs is stronger than for non-intensive InPCE in a similar AMT range. The trends for all seasons have a dropping tail for high AMTs, which could be due to shrinking sample sizes. It could also imply that extreme events (95%) are more influenced by temperature and will likely be more affected by climate change than regular events, a finding that is supported by other researchers (Allen and Ingram, 2002; Trenberth et al., 2003; Allan and Soden, 2008; Giorgi et al., 2011).

Since PD is negatively associated with EPC, intensive (−2000 hPa–−500 hPa) DePCEs contain many extreme events. Seasonality is also more differentiable for intensive DePCEs. A monotonic positive trend between PD and AMT can be observed in fall. In winter, PD increases when the AMT is less than 0 °C, and decreases for warmer temperatures. In spring, PD (except in the 95% percentile) does not obviously change until AMT is > 10 °C. Summer shows a general monotonic decrease in PD as AMT increases. This is consistent with

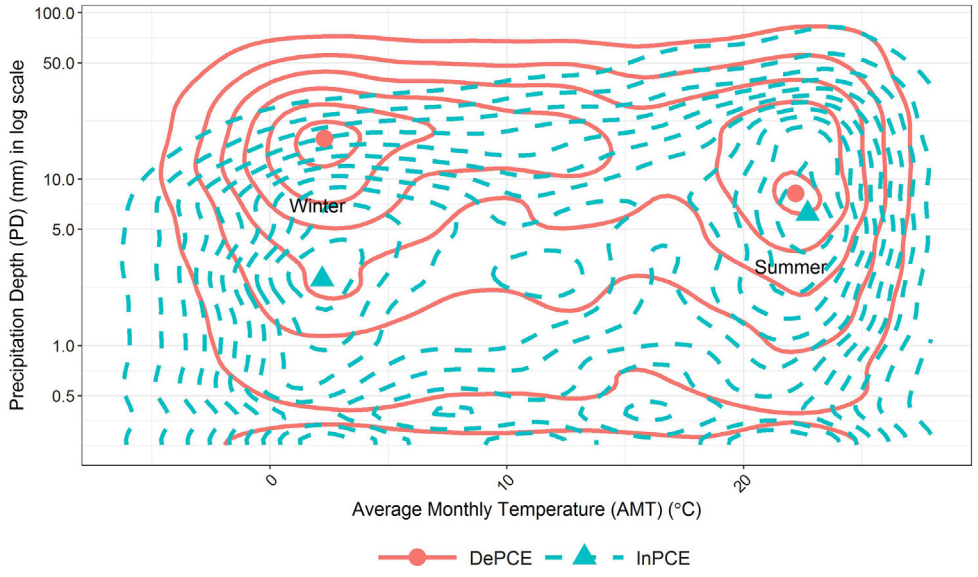

Fig. 10. PD of different PCE types on AMT (red: DePCE, green: InPCE). (For interpretation of the references to colour in this figure legend, the reader is referred to the web version of this article.)

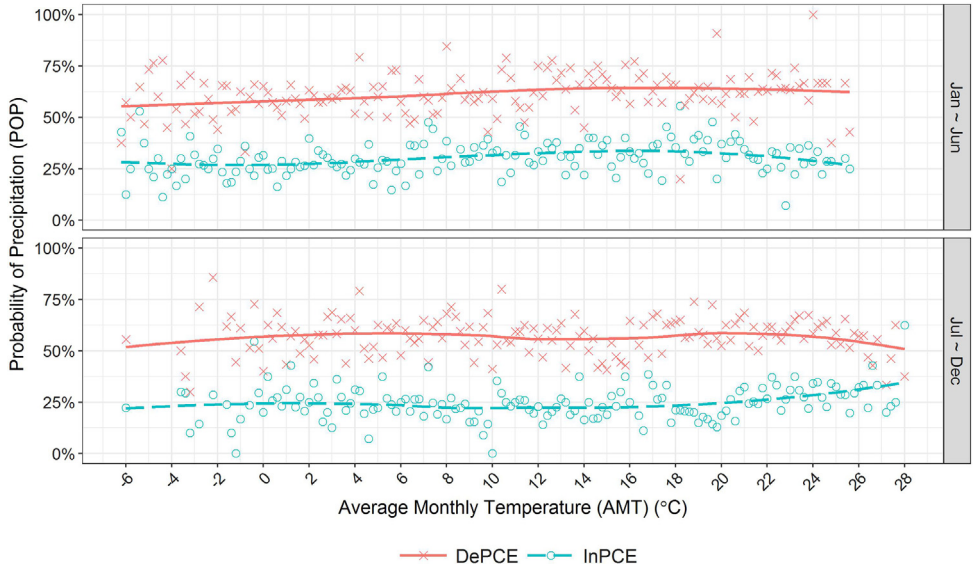

Fig. 11. POP of different PCE types on AMT in different half years (red: DePCE, green: InPCE). (For interpretation of the references to colour in this figure legend, the reader is referred to the web version of this article.)

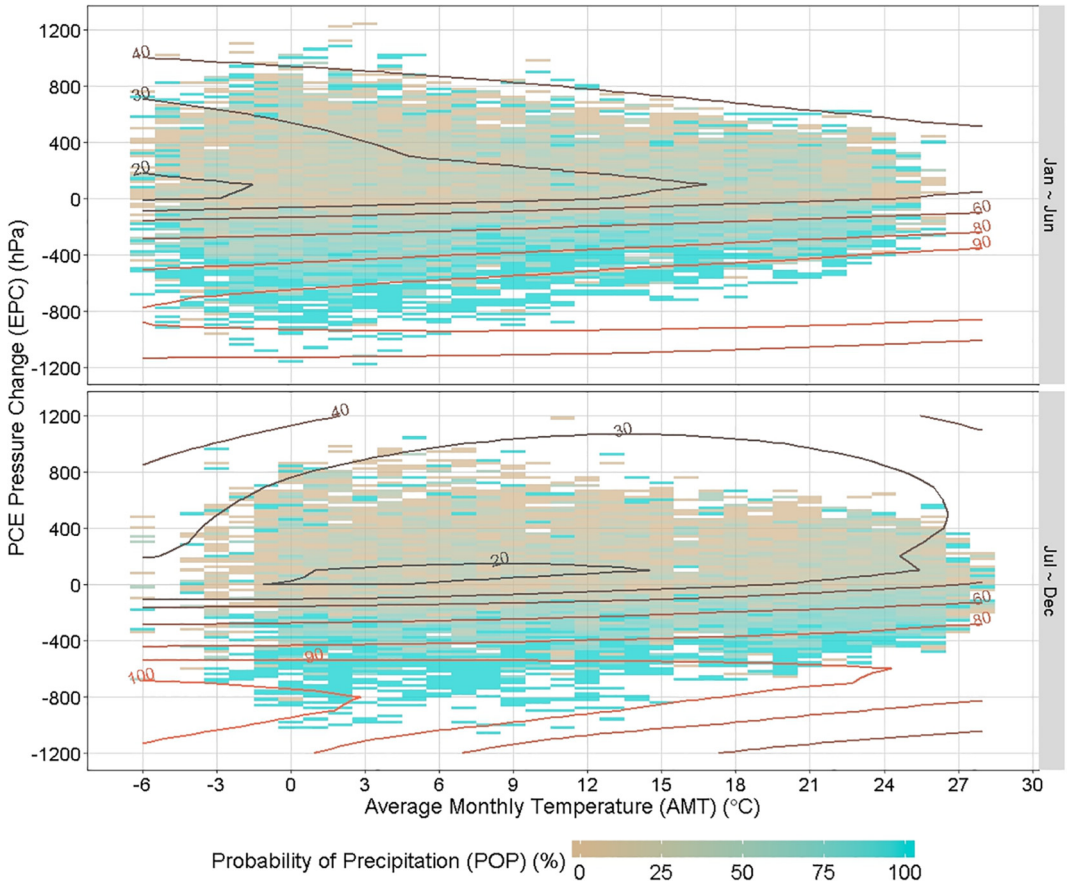

Fig. 12. PCE POP over AMT by EPC.

Shaw et al. (2011)'s findings in the NE, USA, suggesting that extreme precipitation events show a decrease in PD after 25 °C during the summer.

The relationship between PD and AMT is important in the context of downscaling precipitation based on GCM temperature projections, the motivation for this study. AMT could generally indicate the moisture holding capacity and associated non-extreme PD trend of the CC relationship. However, at finer temporal scale or for a specific precipitation event, precipitation should be more physically related to hourly temperature (Panthou et al., 2014; Peleg et al., 2018). Moreover, pressure change, as a driver of precipitation investigated in this study, could impact on PD more directly than temperature and is worth to further explored.

The impacts of both AMT and EPC on precipitation characteristics

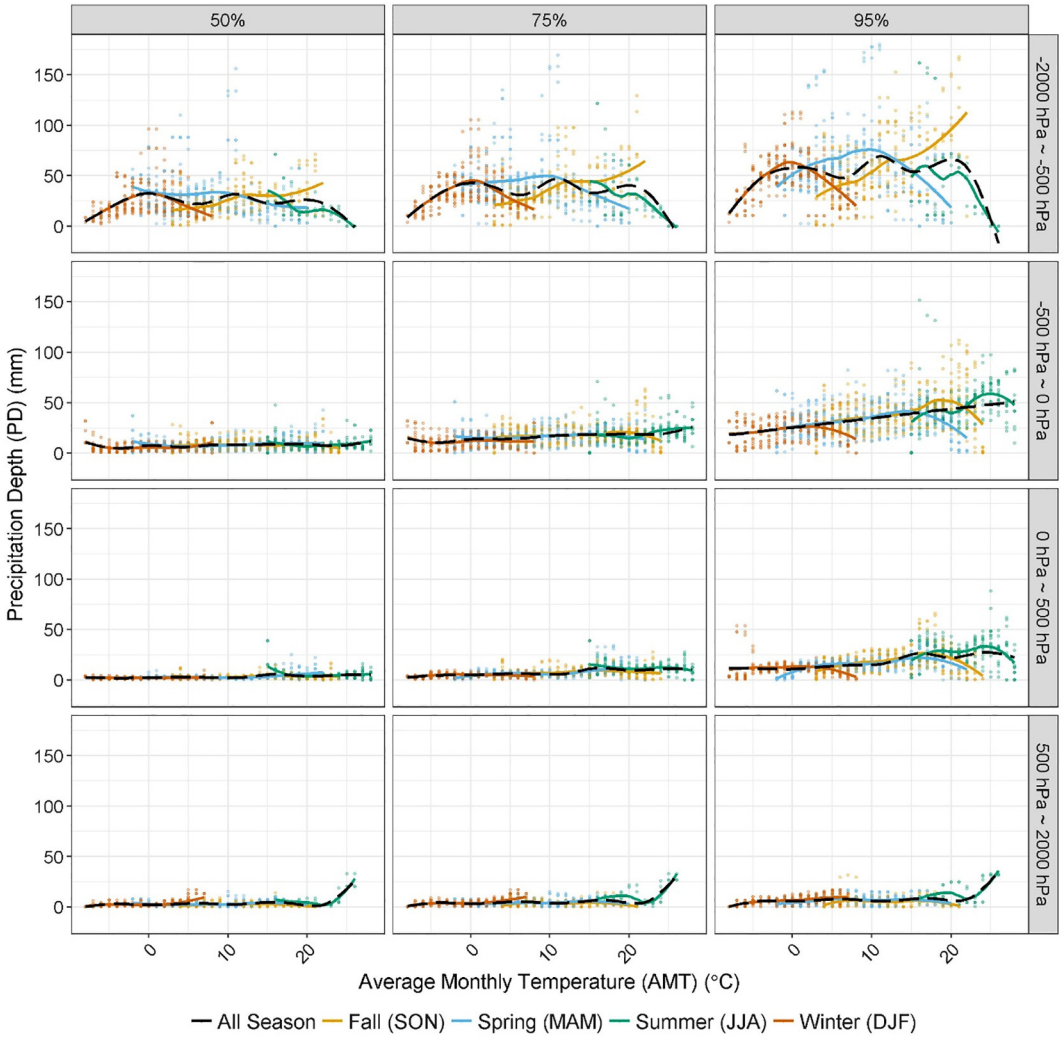

Fig. 13. Seasonal relationship between PD, AMT and EPC in different percentiles.

(POP, PD and percentiles) in Figs. 12 and 13 quantify the precipitation change with climate. Ban et al. (2015) suggest future climate may not be represented by the statistics derived from present using CC-related results. In this study, it might be true for the trends of precipitation characteristics in the extreme situation (e.g. an AMT or an EPC not seen in the historical data, or a local scale summer convection system only shown in the point source data in terms of pressure changes but not precipitation). However, the analysis in this study is not statistical based. Although the intensity of different precipitation types may vary due to divergent thermodynamic conditions across different areal, seasonal and climate conditions (Panthou et al., 2014; Peleg et al., 2018), pressure change as a physical requirement of precipitation formation, described in this study, is independent of global warming. Thus, qualitatively, the dependences between EPC, PD and AMT will be generally held. Meanwhile, the analysis results, for observed climate, may have lower confidence under climate change, especially for local convection events, because a) the sample size of such events is underestimated in the historical data collected by point sources, such as climate stations in this study; b) the trajectory and effective area of precipitation events could change in future climate (Peleg et al., 2018).

5. Conclusion

We investigated the possibility of associating hourly precipitation/pressure data with AMT data as a preliminary analysis for generating a non-stationary, non-parametric, stochastic precipitation generator conditioning GCM monthly temperature output. Specifically, the results of this analysis answer the following two questions: 1) how PD and POP change with EPC during different types of PCE and 2) how the PD and POP of specific PCEs respond to AMT.

Precipitation is formed by the cooling of moist air, typically due to vertical lifting. Physically, this lifting results in reduced sea-level air pressure prior to precipitation events. This research reveals that both POP and PD are highly correlated to PCEs. It provides a more physically reliable strategy by importing pressure change for stochastic precipitation generation, either parameterized statistical type or non-parametric resampling type, to model precipitation. The dependence of precipitation characteristics (POP, PD and percentiles) on AMT and EPC (Figs. 12 and 13) could also enable stochastic precipitation generations to incorporate more reliable GCM AMT projections in generating non-stationary situations. For this reason, we propose a stochastic precipitation generator for generating PCE sequences conditionally, using the corresponding precipitation as an output.

Since the relationship between PCE and precipitation is derived from the physical precipitation formation mechanism, this kind of stochastic precipitation generator represents a much stronger and more reliable conceptual basis on which to build a model, as compared to those models barely relying on statistical assumptions. Moreover, because PCE is more strongly related to precipitation formation than coarser temporal scale temperature (e.g. monthly), it could be a reliable method for downscaling precipitation from GCM AMT projections, which are currently more trustworthy than GCM precipitation

projections. Such a stochastic precipitation generator could be built by sampling PCE-associated hourly precipitation series from historical observations, and by adjusting for GCM predicted monthly temperatures. Specifically, by employing non-parametric method (Lall, Rajagopalan et al., 1996; Lall and Sharma, 1996; Rajagopalan and Lall, 1999), AMT projections from GCMs would be used as a reference to determine a pool of candidate PCEs under similar AMTs (i.e. a range of 6 °C within which POP seasonal changes occur, as shown in Fig. 11), similar to the moving window method (Rajagopalan et al., 1996). A secondary paper, specifically describing such a non-stationary non-parametric stochastic precipitation generator, will be published.

In all, this paper suggests a means of generating long, continuous, synthetic precipitation series from scaled-down GCM AMT projections. These series could then be used for a variety of climate change model applications, such as hydrologic and hydraulic modeling, water resource modeling, agriculture modeling.

Acknowledgements

This research was supported by the National Oceanic and Atmospheric Administration, United States (NOAA) Supporting Regional Implementation of Integrated Climate Resilience: Consortium for Climate Risks in the Urban Northeast (CCRUN) Phase II* (NA15OAR4310147). We thank many colleagues from Drexel University and Columbia University for the insights and expertise they provided which greatly assisted in this research. We also thank for the reviewers' comments that greatly improved the manuscript.

References

Adams-Selin, R.D., Johnson, R.H., 2010. Mesoscale Surface Pressure and Temperature Features Associated with Bow Echoes. Mon. Weather Rev. 138 (1), 212–227.
Ahrens, C.D., 2012. Meteorology Today. Cengage Learning.
Ahrens, C.D., Jackson, P.L., Jackson, C.E.J., Jackson, C.E.O., 2012. Meteorology Today: An Introduction to Weather, Climate, and the Environment. Nelson Education.
Allan, R.P., Soden, B.J., 2007. Large discrepancy between observed and simulated precipitation trends in the ascending and descending branches of the tropical circulation. Geophys. Res. Lett. 34 (18).
Allan, R.P., Soden, B.J., 2008. Atmospheric warming and the amplification of precipitation extremes. Science 321 (5895), 1481–1484.
Allen, M.R., Ingram, W.J., 2002. Constraints on future changes in climate and the hydrologic cycle. Nature 419 (6903), 224.
Ban, N., Schmidli, J., Schär, C., 2015. Heavy precipitation in a changing climate: Does short-term summer precipitation increase faster? Geophys. Res. Lett. 42 (4), 1165–1172.
Basinger, M., Montalto, F., Lall, U., 2010. A rainwater harvesting system reliability model based on nonparametric stochastic rainfall generator. J. Hydrol. 392 (3–4), 105–118.
Bjerknes, J., Kristiania, H.S., 1922. Meteorological conditions for the formation of rain. Q. J. R. Meteorolog. Soc. 48 (204), 374–375.
Bjerknes, J., Kristiania, H.S., 1923. Life cycle of cyclones and the polar front theory of atmospheric circulation. Q. J. R. Meteorolog. Soc. 49 (206), 140–141.
Cleveland, W., Grosse, E., Shyu, W., 1992. Local regression models. In: Chambers, J.M., Hastie, T.J. (Eds.), Statistical Models in S. Chapman & Hall, New York, pp. 309–376.
Dawn, S., Mandal, M., 2014. Surface mesoscale features associated with leading convective line-trailing stratiform squall lines over the Gangetic West Bengal. Meteorol. Atmos. Phys. 125 (3), 119–133.
Defant, A., 1921. Die Veränderungen in der allgemeinen Zirkulation der Atmosphäre in den gemäßigten Breiten der Erde. Geogr. Ann. 3, 209–266.
Demaria, E.M.C., Palmer, R.N., Roundy, J.K., 2016. Regional climate change projections of streamflow characteristics in the Northeast and Midwest U.S. J. Hydrol.: Reg. Stud. 5, 309–323.
Fowler, H.J., Blenkinsop, S., Tebaldi, C., 2007. Linking climate change modelling to impacts studies: recent advances in downscaling techniques for hydrological modelling. Int. J. Climatol. 27 (12), 1547–1578.
Giorgi, F., Im, E.S., Coppola, E., Diffenbaugh, N.S., Gao, X.J., Mariotti, L., Shi, Y., 2011. Higher Hydroclimatic Intensity with Global Warming. J. Clim. 24 (20), 5309–5324.
Groisman, P.Y., Knight, R.W., Easterling, D.R., Karl, T.R., Hegerl, G.C., Razuvaev, V.N., 2005. Trends in Intense Precipitation in the Climate Record. J. Clim. 18 (9), 1326–1350.
Haberlandt, U., von Eschenbach, A.D.E., Buchwald, I., 2008. A space-time hybrid hourly rainfall model for derived flood frequency analysis. Hydrol. Earth Syst. Sci. 12 (6), 1353–1367.
Hayhoe, K., Wake, C., Anderson, B., Liang, X.Z., Maurer, E., Zhu, J.H., Bradbury, J., DeGaetano, A., Stoner, A.M., Wuebbles, D., 2008. Regional climate change projections for the Northeast USA. Mitig. Adapt. Strat. Glob. Change 13 (5–6), 425–436.
Heneker, T.M., Lambert, M.F., Kuczera, G., 2001. A point rainfall model for risk-based design. J. Hydrol. 247 (1), 54–71.
Houze, R.A., Rasmussen, K.L., Zuluaga, M.D., Brodzik, S.R., 2015. The variable nature of convection in the tropics and subtropics: a legacy of 16 years of the Tropical Rainfall Measuring Mission satellite. Rev. Geophys. 53 (3), 994–1021.
Hoxit, L.R., Chappell, C.F., Fritsch, J.M., 1976a. Formation of Mesolows or Pressure Troughs in Advance of Cumulonimbus Clouds. Mon. Weather Rev. 104 (11), 1419–1428.
Hoxit, L.R., Chappell, C.F., Michael Fritsch, J., 1976b. Formation of mesolows or pressure troughs in advance of cumulonimbus clouds. Mon. Weather Rev. 104 (11), 1419–1428.
Hughes, K.K., Mayes, J., 2014. Understanding Weather. Taylor & Francis.
Johnson, F., Sharma, A., 2009. Measurement of GCM Skill in Predicting Variables Relevant for Hydroclimatological Assessments. J. Clim. 22 (16), 4373–4382.
Johnson, F., Sharma, A., 2012. A nesting model for bias correction of variability at multiple time scales in general circulation model precipitation simulations. Water Resour. Res. 48 (1).
Kendon, E.J., Rowell, D.P., Jones, R.G., Buonomo, E., 2008. Robustness of Future Changes in Local Precipitation Extremes. J. Clim. 21 (17), 4280–4297.
King, A.D., Klingaman, N.P., Alexander, L.V., Donat, M.G., Jourdain, N.C., Maher, P., 2014. Extreme Rainfall Variability in Australia: Patterns, Drivers, and Predictability. J. Clim. 27 (15), 6035–6050.
Knupp, K.R., Cotton, W.R., 1985. Convective cloud downdraft structure: an interpretive survey. Rev. Geophys. 23 (2), 183–215.
Kunkel, K.E., Karl, T.R., Brooks, H., Kossin, J., Lawrimore, J.H., Arndt, D., Bosart, L., Changnon, D., Cutter, S.L., Doesken, N., Emanuel, K., Groisman, P.Y., Katz, R.W., Knutson, T., O'Brien, J., Paciorek, C.J., Peterson, T.C., Redmond, K., Robinson, D., Trapp, J., Vose, R., Weaver, S., Wehner, M., Wolter, K., Wuebbles, D., 2013. Monitoring and Understanding Trends in Extreme Storms: State of Knowledge. Bull. Am. Meteorol. Soc. 94 (4), 499–514.
Lall, U., Rajagopalan, B., Tarboton, D.G., 1996. A nonparametric wet/dry spell model for resampling daily precipitation. Water Resour. Res. 32 (9), 2803–2823.
Lall, U., Sharma, A., 1996. A nearest neighbor bootstrap for resampling hydrologic time series. Water Resour. Res. 32 (3), 679–693.
Lenderink, G., van Meijgaard, E., 2008. Increase in hourly precipitation extremes beyond expectations from temperature changes. Nat. Geosci. 1 (8), 511–514.
Lenderink, G., van Meijgaard, E., 2010. Linking increases in hourly precipitation extremes to atmospheric temperature and moisture changes. Environ. Res. Lett. 5 (2).
Madden, R.A., Williams, J., 1978. The Correlation between Temperature and Precipitation in the United States and Europe. Mon. Weather Rev. 106 (1), 142–147.
Meehl, G.A., Arblaster, J.M., Tebaldi, C., 2005. Understanding future patterns of increased precipitation intensity in climate model simulations. Geophys. Res. Lett. 32 (18).
Meehl, G.A., Washington, W.M., Arblaster, J.M., Hu, A., Teng, H., Tebaldi, C., Sanderson, B.N., Lamarque, J.-F., Conley, A., Strand, W.G., W. III, J.B., 2012. Climate System Response to External Forcings and Climate Change Projections in CCSM4. J. Clim. 25 (11), 3661–3683.
Mitchell, J.F.B., Johns, T.C., Eagles, M., Ingram, W.J., Davis, R.A., 1999. Towards the Construction of Climate Change Scenarios. Clim. Change 41 (3), 547–581.
Neiman, P.J., Ralph, F.M., Wick, G.A., Lundquist, J.D., Dettinger, M.D., 2008. Meteorological Characteristics and Overland Precipitation Impacts of Atmospheric Rivers Affecting the West Coast of North America Based on Eight Years of SSM/I Satellite Observations. J. Hydrometeorol. 9 (1), 22–47.
Panthou, G., Mailhot, A., Laurence, E., Talbot, G., 2014. Relationship between Surface Temperature and Extreme Rainfalls: A Multi-Time-Scale and Event-Based Analysis. J. Hydrometeorol. 15 (5), 1999–2011.
Peleg, N., Marra, F., Fatichi, S., Molnar, P., Morin, E., Sharma, A., Burlando, P., 2018. Intensification of convective rain cells at warmer temperatures observed from high-resolution weather radar data. J. Hydrometeorol.
Räisänen, J., 2001. CO2-Induced Climate Change in CMIP2 Experiments: Quantification of Agreement and Role of Internal Variability. J. Clim. 14 (9), 2088–2104.
Rajagopalan, B., Lall, U., 1999. A k-nearest-neighhor simulator for daily precipitation and other weather variables. Water Resour. Res. 35 (10), 3089–3101.
Rajagopalan, B., Lall, U., Tarboton, D.G., 1996. Nonhomogeneous Markov Model for Daily Precipitation. J. Hydrol. Eng. 1 (1), 33–40.
Restrepo-Posada, P.J., Eagleson, P.S., 1982. Identification of independent rainstorms. J. Hydrol. 55 (1), 303–319.
Rodriguez-Iturbe, I., Cox, D.R., Isham, V., 1987. Some Models for Rainfall Based on Stochastic Point Processes. Proc. R. Soc. Lond. Ser. A Math. Phys. Sci. 410 (1839), 269–288.
Rodriguez-Iturbe, I., Cox, D.R., Isham, V., 1988. A Point Process Model for Rainfall: Further Developments. Proc. R. Soc. Lond. Ser. A Math. Phys. Sci. 417 (1853), 283–298.
Shamir, E., Megdal, S.B., Carrillo, C., Castro, C.L., Chang, H.-I., Chief, K., Corkhill, F.E., Eden, S., Georgakakos, K.P., Nelson, K.M., Prietto, J., 2015. Climate change and water resources management in the Upper Santa Cruz River, Arizona. J. Hydrol. 521 (Supplement C), 18–33.
Sharma, A., Lall, U., 1999. A nonparametric approach for daily rainfall simulation. Math. Comput. Simul. 48 (4–6), 361–371.
Shaw, S.B., Royem, A.A., Riha, S.J., 2011. The Relationship between Extreme Hourly Precipitation and Surface Temperature in Different Hydroclimatic Regions of the United States. J. Hydrometeorol. 12 (2), 319–325.
Sorteberg, A., KvamstØ, N.G., 2006. The effect of internal variability on anthropogenic climate projections. Tellus A 58 (5), 565–574.
Stern, R.D., Coe, R., 1984. A Model Fitting Analysis of Daily Rainfall Data. J. R. Stat. Soc. Ser. A (Gen.) 147 (1), 1–34.
Sun, Y., Solomon, S., Dai, A., Portmann, R.W., 2007. How often will it rain? J. Clim. 20

(19), 4801–4818.
Trenberth, K.E., 1998. Atmospheric moisture residence times and cycling: implications for rainfall rates and climate change. Clim. Change 39 (4), 667–694.
Trenberth, K.E., 2011. Changes in precipitation with climate change. Clim. Res. 47 (1–2), 123–138.
Trenberth, K.E., Dai, A., Rasmussen, R.M., Parsons, D.B., 2003. The changing character of precipitation. Bull. Am. Meteorol. Soc. 84 (9), 1205.
Trenberth, K.E., Shea, D.J., 2005. Relationships between precipitation and surface temperature. Geophys. Res. Lett. 32 (14).
Urbana-Champaign, W. W. W. a. t. U. o. I. a., 2010. Occluded Front. from http://ww2010.atmos.uiuc.edu/%28Gh%29/guides/mtr/af/frnts/ofdef.rxml.
USGCRP, 2017. Climate Science Special Report: Fourth National Climate Assessment, Volume I. D. J. Wuebbles, D. W. Fahey, K. A. Hibbard et al. U.S. Global Change Research Program, Washington, DC, USA, p. 470.
Wasko, C., Pui, A., Sharma, A., Mehrotra, R., Jeremiah, E., 2015a. Representing low-frequency variability in continuous rainfall simulations: A hierarchical random Bartlett Lewis continuous rainfall generation model. Water Resour. Res. 51 (12), 9995–10007.
Wasko, C., Sharma, A., 2017. Continuous rainfall generation for a warmer climate using observed temperature sensitivities. J. Hydrol. 544 (Supplement C), 575–590.
Wasko, C., Sharma, A., Johnson, F., 2015b. Does storm duration modulate the extreme precipitation-temperature scaling relationship? Geophys. Res. Lett. 42 (20), 8783–8790.
Westra, S., Alexander, L.V., Zwiers, F.W., 2013. Global Increasing Trends in Annual Maximum Daily Precipitation. J. Clim. 26 (11), 3904–3918.
Wilks, D.S., 1998. Multisite generalization of a daily stochastic precipitation generation model. J. Hydrol. 210 (1), 178–191.
Wilks, D.S., 2010. Use of stochastic weather generators for precipitation downscaling. Wiley Interdisciplinary Rev.-Clim. Change 1 (6), 898–907.
Wilks, D.S., Wilby, R.L., 1999. The weather generation game: a review of stochastic weather models. Prog. Phys. Geogr. 23 (3), 329–357.
Zhao, W., Khalil, M.A.K., 1993. The Relationship between Precipitation and Temperature over the Contiguous United States. J. Clim. 6 (6), 1232–1236.
Zveryaev, I.I., Allan, R.P., 2005. Water vapor variability in the tropics and its links to dynamics and precipitation. J. Geophys. Res. Atmos. 110(D21).